ONLINE DATA SUPPLEMENT

Targeted Immune and Growth Factor Proteomics of Right Heart Adaptation to Pulmonary Arterial Hypertension

Myriam Amsallem MD PhD[a,b,c*], Andrew J. Sweatt MD[c,d*], Jennifer Arthur Ataam PhD[a,b], Julien Guihaire MD PhD[e], Florence Lecerf MS[e], Mélanie Lambert PhD[e], Maria Rosa Ghigna MD PhD[f], Md Khadem Ali PhD[c,d], Yuqiang Mao MD PhD [c,d], Elie Fadel MD PhD[e], Marlene Rabinovitch MD[c,g], Vinicio de Jesus Perez MD PhD[c,d], Edda Spiekerkoetter MD[c,d], Olaf Mercier MD PhD[e], Francois Haddad MD[a,b,c*], Roham T. Zamanian MD[c,d*]

Supplementary Methods

1) Plasma sample collection, processing and biorepository storage

Pulmonary arterial hypertension. PAH samples were obtained from the Stanford Pulmonary Hypertension Biobank (Stanford University, CA, USA), which is a comprehensive tissue bank that includes plasma, serum, peripheral blood mononuclear cells, exhaled breath condensate, and urine from patients with all forms of pulmonary hypertension (Stanford University IRB #14083). Initiated in 2007, the Stanford Pulmonary Hypertension Biobank has captured samples from over 600 well-characterized subjects who were recruited at the time of evaluation in Stanford Pulmonary Hypertension clinic. After informed consent was obtained, study plasma samples were collected from patients during right heart catheterization in the fasting state. Peripheral blood was drawn from the antecubital fossa into EDTA vacutainers under standard sterile precautions. Collection tubes were immediately placed upright into a rack at room temperature. Within 30 minutes, the sample was inverted several times to mix components, and subsequently centrifuged at 1300 rpm for 10 minutes. The plasma layer was then carefully removed by pipette without disturbing the buffy coat, and transferred to Eppendorf tubes in 200µL aliquots.

Aliquoted samples were secured and stored upright at -80°C in the Stanford Pulmonary Hypertension Biobank.

Healthy controls. Control plasma samples (n=88) were acquired from the Stanford Cardiovascular Institute Biomarker and Phenotype Core Laboratory biorepository (Stanford University #40869). Samples were collected from healthy volunteers between 2009 and 2013, as part of the Stanford Healthy Aging Study (Stanford University IRB #20942). Peripheral venous blood was drawn in the fasting state from the antecubital fossa, and subsequently processed and stored utilizing the same protocol and conditions that were applied for PAH samples (see above). To establish health in these individuals, initial screening involved a comprehensive questionnaire and clinical assessment with blood pressure and anthropometric measurements. Subjects were excluded for any unexplained chronic cardiopulmonary symptoms (dyspnea, cough, angina, palpitations, orthopnea, lightheadedness), symptomatic atherosclerotic disease, symptomatic heart failure, history of atrial fibrillation, hypertension, chronic pulmonary disease, diabetes mellitus requiring therapy, current smoking, hyperlipidemia requiring therapy, body mass index above 35kg/m2, history of atopy, chronic systemic inflammatory disease, recent infectious disease, prior or current malignancy, and Alzheimer's disease. Subjects had basic laboratory studies to rule out dyslipidemia, elevated NT-proBNP (above or equal to 300 pg/mL), abnormal liver function tests, and renal dysfunction (stage 3 or greater). The participants were then screened with vascular ultrasound for abdominal aortic aneurysm (5cm or greater) and asymptomatic carotid or femoral atherosclerosis (20% or greater diameter stenosis). Transthoracic echocardiography was also employed to screen and exclude those with subclinical left ventricular dysfunction (ejection fraction <50%), subclinical valvular heart disease

(categorized as mild or greater), any right ventricular enlargement or dysfunction, or estimated right ventricular systolic pressure 30mmHg or greater).

2) Multiplex immunoassay blood proteomic profiling

Immunoassay sample and plate preparation. The Luminex 200™ plate reader instrument was calibrated according to manufacturer instructions. This process employed Bio-Plex calibration beads to standardize fluorescent signal detection. To prepare experimental samples, frozen biobanked plasma aliquots were passively thawed to room temperature and diluted four-fold in assay buffer (1 volume plasma to 3 volumes buffer). These plasma samples were assayed within 30 minutes of reaching room temperature, as described below. To prepare a magnetic capture bead mixture, bead stock solution (20x) was vortexed at medium speed for 30 seconds and then diluted 20-fold in assay buffer. The preparation of standards involved first adding 500⌈L of standard diluent to each stock vial of lyophilized standard, which contained known concentrations of analytes measured by our assay. The reconstituted standard was vortexed and incubated on ice for 30 minutes. Thereafter, we performed four-fold serial dilution to prepare a series of eight total standards.

Immunoassay execution. After preparation of the samples, capture bead mixture, and standards, the immunoassay was carried out on a 96-well plate. First, we added 75⌈L of standard to eight wells (one standard dilution per well), 75⌈L of assay buffer to one well (‘blank’ well without sample later used to measure background fluorescence from non-specific binding), and a 75⌈L pre-diluted experimental sample to the remaining wells. Next, we added 25⌈L of capture bead mixture to all plate wells. The plate was sealed, placed on a shaker for two hours (800 rpm), and incubated at 4°C overnight. After passive re-warming the next day, solution was removed and

the plate was washed by magnetic separation with the Bio-Plex Pro™ wash station (200 ⌈L buffer, 3 cycles). Biotinylated detection antibody stock solution (10x) was diluted 10-fold in assay buffer and added to each well (25 ⌈L), followed by two-hour incubation on a shaker (800 rpm), solution removal, and three magnetic separation washes. Next, streptavidin-phycoerythrin stock solution (100x) was diluted 100-fold, incubated in each well (50 ⌈L) for 40 minutes on a shaker (500 rpm), removed, and the plate was washed again. Finally, after addition of reading buffer (100 ⌈L) and ten-minute incubation on a shaker (800 rpm), the plate was read by a Luminex 200™ dual-laser detection instrument. Data acquisition was set to a 50-bead count minimum per analyte per well. Data was processed and presented with Bio-plex Manager™ software.

3) Echocardiographic RV phenotyping of PAH patients

Digitized echocardiographic studies were acquired by the Stanford Biomarker and Phenotypic Laboratory, using Philips IE 33 ultrasound systems (Philips, Amsterdam, The Netherlands). All measures were averaged over three cycles, performed according to the latest American Society of Echocardiography guidelines (22,23) and assessed off-line by two blinded certified readers, as recently described (3). Right heart dimensions and functional metrics were measured on RV-focused apical 4-chamber views (24). RV end-systolic area was indexed on ideal body weight-adjusted body surface area (RVESAI). RV end-systolic remodeling index (RVESRI) was defined by the lateral wall to septal height ratio (3). RV function was assessed using free-wall Lagrangian longitudinal strain (RVLS, measured from mid-endocardial end-diastolic and end-systolic manually traced lengths), RV fractional area change (RVFAC) and tricuspid annular plane systolic excursion (TAPSE).

Follow-up echocardiograms available in survivors at 1 year were available in 174 patients (93% of 1-year survivors). These echocardiograms were interpreted using the same methodology. Right heart remodeling with therapy was defined using changes in RVESRI from baseline echocardiograms, as previously published in Amsallem et al. Circulation Cardiovascular Imaging, 2017 (1). Improvement in RVESRI was defined by a relative delta <10% between the baseline and follow-up echo, worsening if >10% and stable otherwise. Binary logistic regression analyses were used to assess whether baseline levels of HGF, NGF, SCGFb or SDF1 were associated with the end point of improvement in RVESRI at 1 year. To explore the predictive value of these biomarkers stratifying on the therapy initiated or changes in PH-specific therapy between baseline and follow-up, we performed binary logistic regression analyses in the three following subgroups: [1] patients in whom parenteral prostanoids were initiated between baseline and follow-up, [2] patients in whom there was no change in PH-specific therapies (including ERA, PDE5I, or oral prostanoids) and [3] others.

4) Histological analysis of human RV tissue

Right ventricular myocardial samples from the 4 patients with PAH were embedded in paraffin for histological study. They were cut in 4 μm-thick sections and stained with 0.1% Picro-Sirius Red for histological evaluation of fibrosis on a single slice. Histological image processing was performed using Nikon NIS-Elements (Tokio, Japan). Quantification of fibrosis from histological images was performed using semi-automated segmentation through a multi-channel thresholding method based on the color and illumination contents (using ImageJ software v.1.4, NIH, Bethesda, MD). The histology images were first manually determined by outlines, which defined each tissue component separately. Artifacts and objects of non-interest (background,

perivascular, endocardial fibrosis, and epicardial fibrosis) were manually delineated from the selected area. The quantitative results were expressed as the surface area for myocardium and fibrosis.

5) Western blots: protein quantification in human RV tissue

Western blots were performed on frozen samples from right ventricles of 4 patients with PAH and 5 controls to compare protein levels of the 4 biomarkers (HGF, NGF, SCGFbeta or SDF1) or their known receptors (c-Met, TrkA). RV biopsies were lysed and sonicated in RIPA buffer supplemented with protease/phosphatase inhibitor cocktail. Following agitation for 1h at 4°C, the lysate was obtained after centrifugation at 4000 g for 10 minutes at 4°C. Protein concentration in lysates was determined by BCA protein assay kit (Thermo Scientific, Rockford, IL); 40 µg of total proteins were separated on 4–20% sodium dodecyl sulfate-polyacrylamide gel electrophoresis gels (Criterion, Biorad). Proteins were transferred to polyvinylidene difluoride or nitrocellulose membranes (Hybond, Amersham) and blocked for 1 hour at room temperature with 5% nonfat dry milk in Tris-buffered saline plus 0.1% Tween 20. Incubation with specific primary antibodies presented in the table below was performed in a blocking buffer overnight at 4°C. Horseradish peroxidase–conjugated anti-mouse IgG (7076, cell signaling) or anti-rabbit IgG (7074, cell signaling) was used as secondary antibody and incubate 1h, in blocking buffer, at room temperature. Immunoreactive bands were detected using ECL chemiluminescent substrate (RPN2236, amersham). Membrane stripping was done by incubating the membrane in Restore Western blot stripping buffer (Thermo Scientific) according to the manufacturer's instructions. Relative expression was expressed by normalizing the protein of interest to the Glyceraldehyde 3-phosphate dehydrogenase (GAPDH).

Anticorps	Species	Reference	Dilution
anti-HGF polyclonal antibody	Rabbit	ab83760, Abcam	1/1000
Recombinant anti-c-Met antibody	Rabbit	ab51067, Abcam	1/1000
anti-NGF antibody	Rabbit	ab6199, Abcam	1/500
recombinant anti-TrkA antibody	Rabbit	ab76291, Abcam	1/500
anti-SDF1 polyclonal antibody	Rabbit	ab9797, Abcam	1/1000
anti-SCGFb antibody	Mouse	ab90238, Abcam	1/250

Incubation with specific primary antibodies (all Abcam, Cambridge, UK): anti-HGF polyclonal antibody (ab83760), recombinant anti-c-Met antibody (ab51067), anti-NGF antibody (ab6199), recombinant anti-TrkA antibody (ab76291), anti-SDF1 polyclonal antibody (ab9797) and anti-SCGFβ antibody (ab90238) were performed in blocking buffer overnight at +4°C. Horseradish peroxidase–conjugated anti-IgG was used as a secondary antibody. Immunoreactive bands were detected by ECL chemiluminescent substrate (Perkin Elmer). If needed, membrane stripping was done by incubating the membrane in the Restore Western blot stripping buffer (Thermo Scientific) according to the manufacturer's instructions. Relative expression was expressed by normalizing the protein of interest to the Glyceraldehyde 3-phosphate dehydrogenase (GAPDH).

6) Immunofluorescence: protein localization in human RV tissue

Paraffin embedded RV slices (5 µm) were deparaffinized in toluene and rehydrated in baths of decreasing concentration of ethanol, prior to water baths. Then unmasking was performed using

two unmasking baths with different pH (pH6 or pH9), depending on the primary antibody used. Sections were saturated with BSA (0.1%) and goat serum (10%), diluted in PBS, for 1 h at room temperature. They were then incubated overnight at 4°C with the primary antibodies presented in the table below, washed with PBS, before incubation with the secondary antibody presented in table 2, 1h at room temperature. Slides were counterstained with 4',6'-diamidino-2-phenylindole (DAPI). Each slide was visualized with a confocal microscope Zeiss (LSM 800) and processed with ZEN software (Carl Zeiss Microscopy, NY, USA).

Anticorps	**Species**	**Reference**	**Dilution**	**pH of unmasking bath**
Anti-HGF polyclonal antibody	Rabbit	ab83760, Abcam	1/100	9
Recombinant anti-c-Met antibody	Rabbit	ab51067, Abcam	1/100	9
Anti-NGF antibody	Rabbit	ab6199, Abcam	1/100	6
Recombinant anti-TrkA antibody	Rabbit	ab76291, Abcam	1/100	9
Anti-SDF1 polyclonal antibody	Rabbit	ab9797, Abcam	1/100	6

Anti-SCGFb antibody	Mouse	ab90238, Abcam	1/100	9
Anti-CD31 antibody	Mouse	M0823, Clone JC70A, Dako	1/50	6 & 9
Anti-CD31 antibody	Rabbit	ab28364, Abcam	1/50	9
Anti-CD68 antibody	Mouse	ab955, Abcam	1/100	6 & 9
Anti-CD68 antibody	Rabbit	ab125212, Abcam	1/100	9
Anti-Vimentin antibody	Mouse	ab8978, Abcam	1/100	6 & 9
Anti-TNNT2	Mouse	A25969, life technologies	1/50	6 & 9
Anti-α-SMA -FITC	Mouse	clone 1A4, Sigma-Aldrich	1/400	6 & 9
Anti-rabbit (594)	Goat	A11037, invitrogen	1/400	6 & 9
Anti-mouse (594)	Goat	A11032, invitrogen	1/400	6 & 9

Anti-rabbit (488)	Goat	A11034, invitrogen	1/400	6 & 9
Anti-mouse (488)	Goat	A11029, invitrogen	1/400	6 & 9

7) Pulmonary arterial banding (PAB) mouse experimental model

All animal experiments were performed in accordance with National Research Council guidelines (*Guide for Care and Use of Laboratory Animals*) and approved by local authorities (APLAC, Stanford University, Protocol #27626). Experiments were conducted in a blinded fashion whenever possible (i.e. exercise testing, haemodynamics measurements, or histological analysis). The PAB model was established to induce chronic RV pressure overload in 10-14-week-old male C57BL/6 mice, as previously published (2). All mice were anesthetized with 0.05–0.1 mg/mg Buprenorphine subcutaneously along with continuous Isoflurane (2–3%). A left thoracotomy was performed at the fourth intercostal space, and the main pulmonary artery was exposed with and banded around a 24G needle with 6-0 silk sutures. Maintenance anesthesia was performed using 1% to 2% isoflurane. The sham surgery control group consisted of age-matched littermates who underwent the same procedure, including isolation of the pulmonary artery trunk without placing a suture. One week after surgery, a peak pressure gradient was measured across the PA band with echocardiography (GE Vivid 7) and only mice with peak pressure gradient >15 mmHg were included into the study protocol. After 5 weeks of surgery, pulmonary artery pressure, heart rate, pulmonary valve velocity time integral by echocardiography were measured to document a reduced cardiac output (2), and RV tissues were collected and snap frozen for further use.

8) Gene expression analysis of PAB model RV samples

Total RNA was isolated from homogenized RV of the PAB model using the RNAeasy Plus Kit (Qiagen, Hilden, Germany) and then reverse transcribed into cDNA using SuperScript III (Invitrogen, Carlsbad, CA, USA) according to the manufacturer's instructions. The level of mRNA transcripts for *Hgf*, *c-Met*, *Ngf*, *Scgfβ* were measured in triplicate using a reaction mixture containing TaqMan gene expression master mix and primer/probe sets (Applied Biosystems, Foster City, CA, USA) and normalized to GAPDH (2).

10) Statistical analysis: Partial least squares regression

Partial least squares (PLS) regression overview. PLS regression was chosen given that it can handle a large number of predictor variables and multiple correlated predictors. Several proteomic blood biomarkers were measured (predictors in this study) including mainly cytokines and chemokines, which inherently often exhibit multicollinearity. Briefly, PLS regression involves the extraction of several linear combinations of the predictor variables, called latent factors, which maximize covariance between predictors and the response variable. In other words, the PLS approach finds latent factors which account for as much variation in the predictors as possible while still modeling the response variable. Proteomic data preprocessing involved background fluorescence subtraction, plate/batch adjustment (empirical Bayes methodology) [11], robust quantile normalization, and duplicate averaging, and adjustment for age, sex, and body mass index.

PLS regression implementation. PLS multivariate regression was carried out using the 'pls' R software package (3). PLS models were fit using the SIMPLS algorithm. The SIMPLS method, compared to other PLS algorithms, truly attempts to maximize the covariance criterion when

determining latent factors, and obeys orthogonality and normalization restrictions. SIMPLS analysis avoids the construction of deflated data matrices and is easily interpretable. PLS models were fit to associate measured proteomic predictors with various response variables: Mayo right heart score, Stanford right heart score, individual components of these right heart scores (RVLS, NYHA functional class, NT-proBNP, and RVESRI), and pulmonary hemodynamic measures (mPAP and PVR). Each PLS regression model consisted of the full matrix of proteomic predictors and a right heart score, single RV metric, or clinical response variable. First, models were fit with the full number of components and a leave-one-out cross validation procedure. To select the optimal number of components for inclusion in each model, we evaluated the root mean squared error of prediction (RMSEP) as a function of number of components, and the one-sigma heuristic was applied (4). Then, each model was fit with the fewest number of components that minimized RMSEP. To identify the RHMP proteomic markers, we focused on the models in which the Mayo Clinic right heart score and Stanford right heart score were the response variable. The most significant predictors were identified from (i) variable importance for projection (VIP) scores and regression beta coefficients. VIP scores quantified the importance of each protein marker in the construction of latent factors. Significance testing was performed for the regression coefficients, by using jackknife resampling to obtain coefficient variance estimates and then applying t-tests.

Figure E1. Volcano plots of the partial least square regression analyses of the circulating proteomic biomarkers associated with right heart scores and metrics in both cohorts. The y-axis represents the VIP scores and the x-axis the Spearman correlation coefficient. Red: higher cytokine levels correlate with less favorable risk score or right heart metric (as continuous variables). Green: higher cytokine levels correlate with a more favorable risk score or right heart metric. MPAP: mean pulmonary arterial hypertension; NYHA: New York Heart Association; PVR: pulmonary vascular resistance; RVLS: right ventricular free-wall longitudinal strain is presented in absolute value (lowest values indicate worst right ventricular dysfunction); RVESRI: right ventricular end-systolic remodeling index. For cytokines abbreviations, please see **Table E1**.

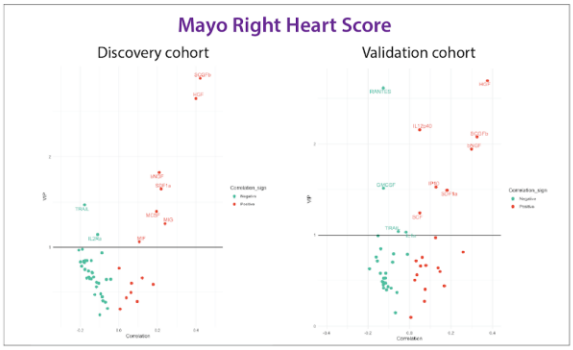
Mayo Right Heart Score
Discovery cohort
Validation cohort

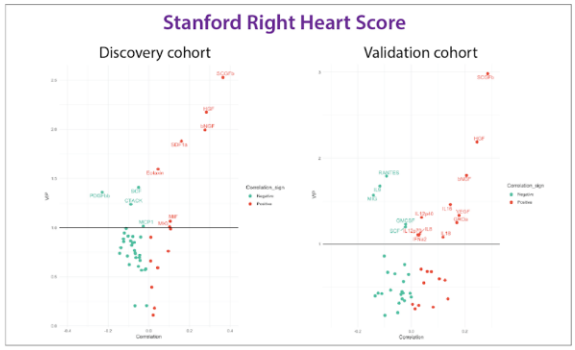
Stanford Right Heart Score
Discovery cohort
Validation cohort

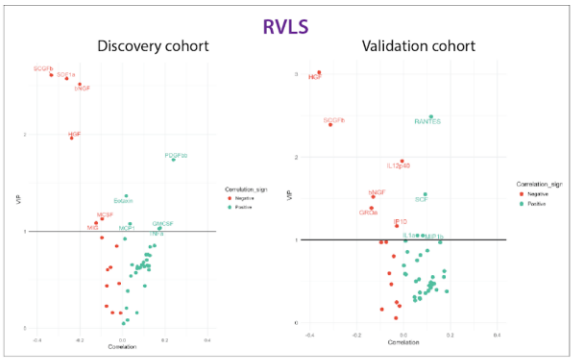
RVLS
Discovery cohort
Validation cohort

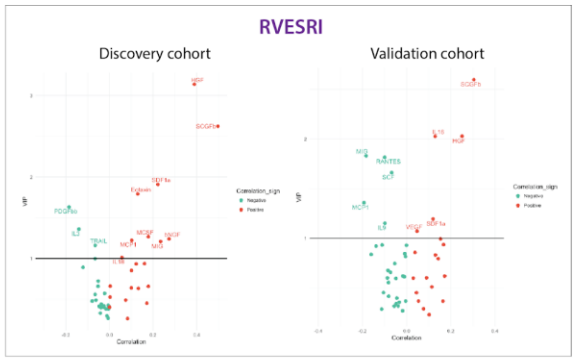
RVESRI
Discovery cohort
Validation cohort

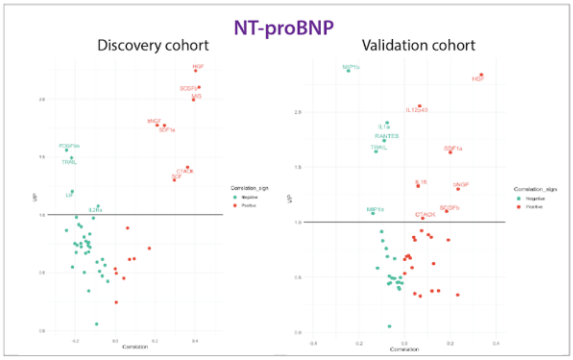
NT-proBNP
Discovery cohort
Validation cohort

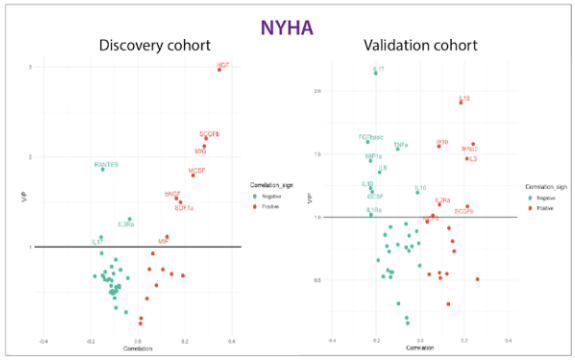
NYHA
Discovery cohort
Validation cohort

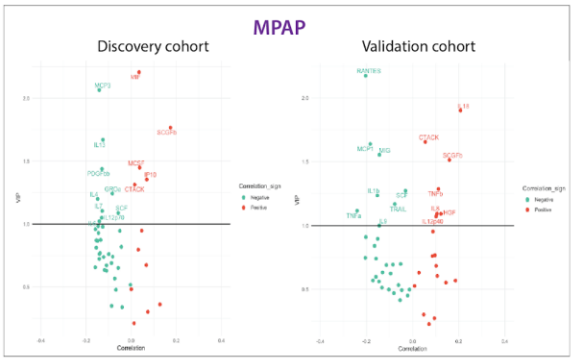
MPAP
Discovery cohort
Validation cohort

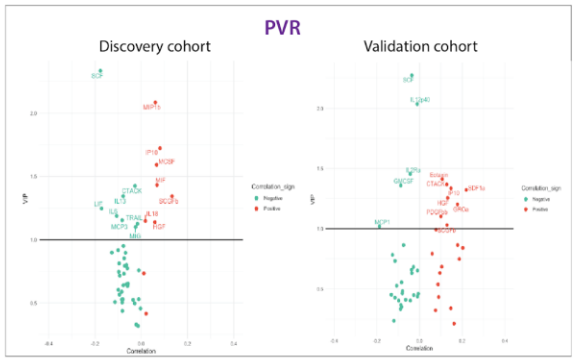
PVR
Discovery cohort
Validation cohort

Figure E2. Levels of the 4 markers according to gender (a) or ethnicity and race (b). (a) Comparative analyte levels of the 4 biomarkers associated with right heart maladaptive phenotype according to gender in healthy controls (n=88) and in patients with PAH (n=197), using Kruskal Wallis test with post-hoc pairwise comparisons adjusted for multiple testing (Benjamini Hochberg). Male versus female comparison p-values are shown among controls and PAH subjects. **(b)** Comparative analyte levels of the 4 strongest biomarkers associated with right heart maladaptive phenotype according to ethnicity and race groups in the total cohort of patients with PAH (n=197), using Kruskal Wallis test (across-groups) with post-hoc pairwise comparisons adjusted for multiple testing (Benjamini Hochberg). For each marker, the across-group p-value is shown along with only significant ($p<0.05$) pairwise comparisons. The p-values for all other pairwise comparisons not shown were non-significant.

a)

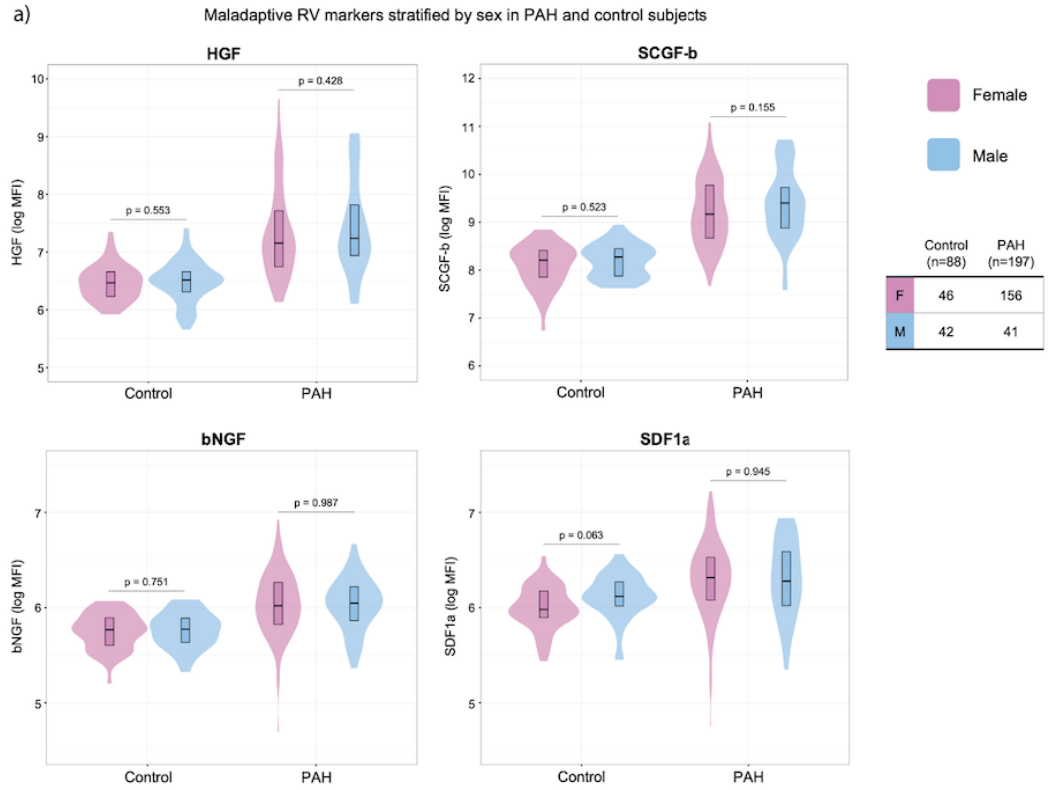

	Control (n=88)	PAH (n=197)
F	46	156
M	42	41

b)

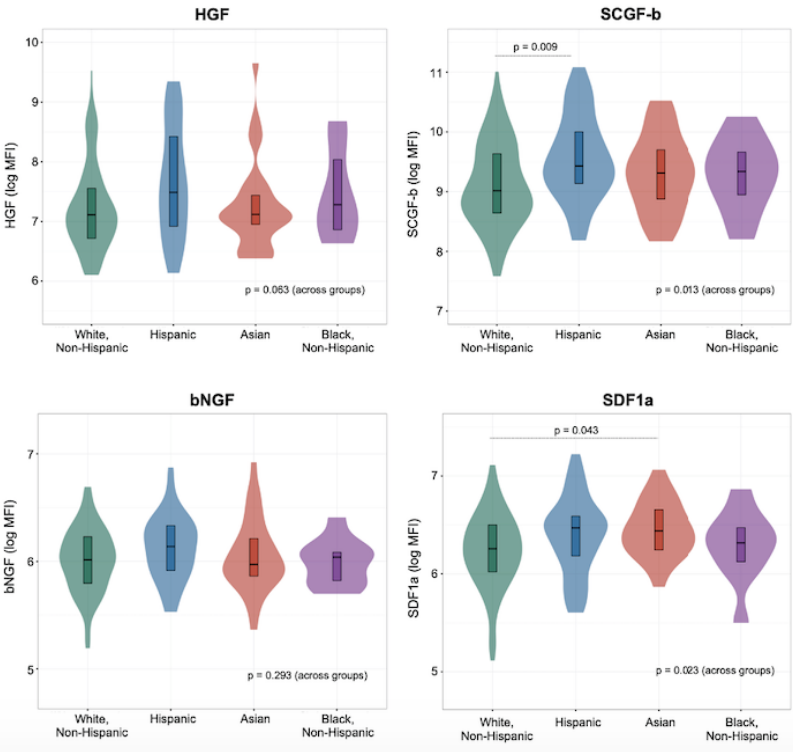

Race	n (%)
White, non-Hispanic	113 (57.4%)
Hispanic	35 (17.8%)
Asian	29 (14.7%)
Black, non-Hispanic	10 (5.1%)
Other	10 (5.1%)

Figure E3. Five-year Kaplan Meier survival curves for the primary combined end point of death, lung transplant or hospitalization for acute right heart failure according to quartiles of stem cell growth factor beta (SCGFβ) levels at baseline.

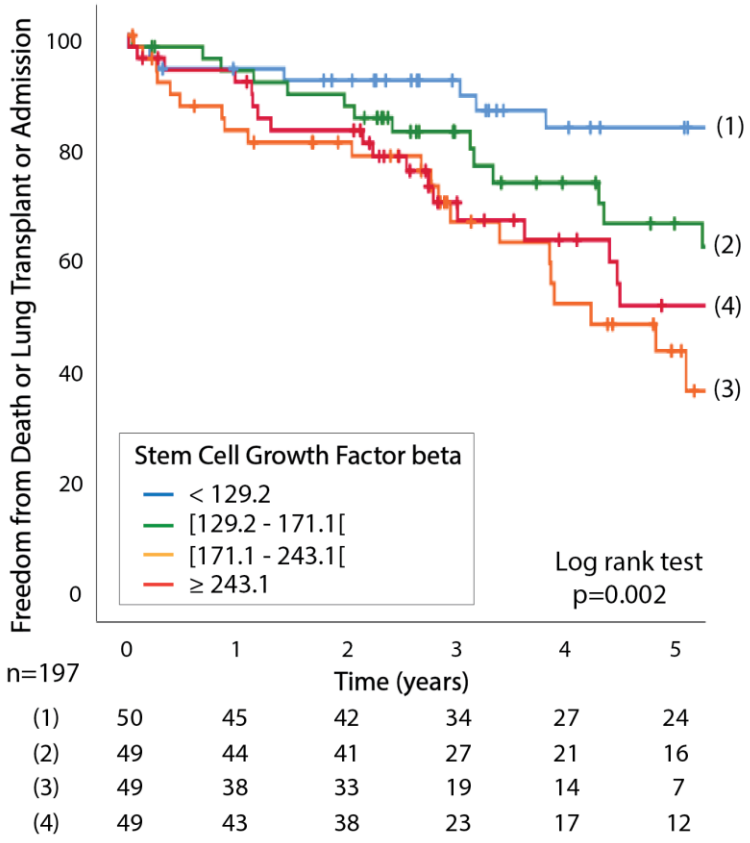

n=197						
(1)	50	45	42	34	27	24
(2)	49	44	41	27	21	16
(3)	49	38	33	19	14	7
(4)	49	43	38	23	17	12

Figure E4. Illustrative right ventricular myocardial biopsies from patients with either idiopathic (left panel) or BMPR2 mutation-related pulmonary arterial hypertension PAH (right panel). Fibrosis levels were measured after Picro-Sirius Red staining, and expressed as the ratio between fibrosis and the total amount of tissue assessed (by determining the total tissue areas occupied by cardiomyocytes and collagen, excluding the lumen). Quantification of fibrosis from histological images was performed using semi-automated segmentation through a multi-channel thresholding method based on the color and illumination contents (using ImageJ software v.1.4, NIH, Bethesda, MD).

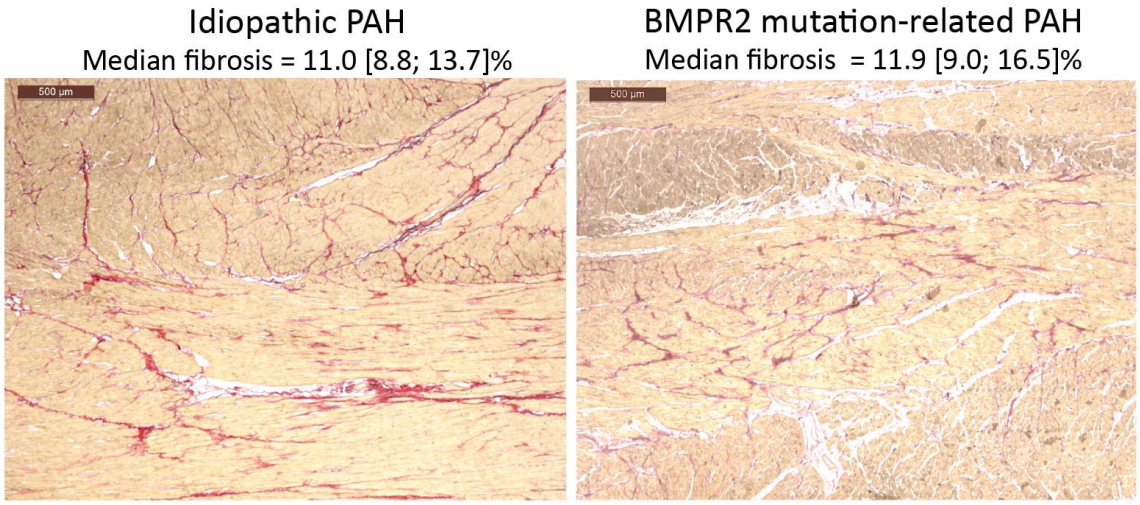

Figure E5. Localization of TrkA (A, red) and its ligand NGF (B, red), SCGFb (C, red) or SDF1 (D, red) in right ventricular biopsies from a patient with idiopathic pulmonary arterial hypertension by immunostaining, double-labeled with either troponin TNNT2 (cardiomyocyte), α-SMA (smooth muscle cell), CD31 (endothelial cells), vimentin VMTN (fibroblast) or CD68 (macrophage) in green, from left to right. No immunoreactivity was seen in cells incubated with the secondary antibody but no primary antibody. Scale bar = 10 μm. DAPI = 4′,6′-diamidino-2-phenylindole.

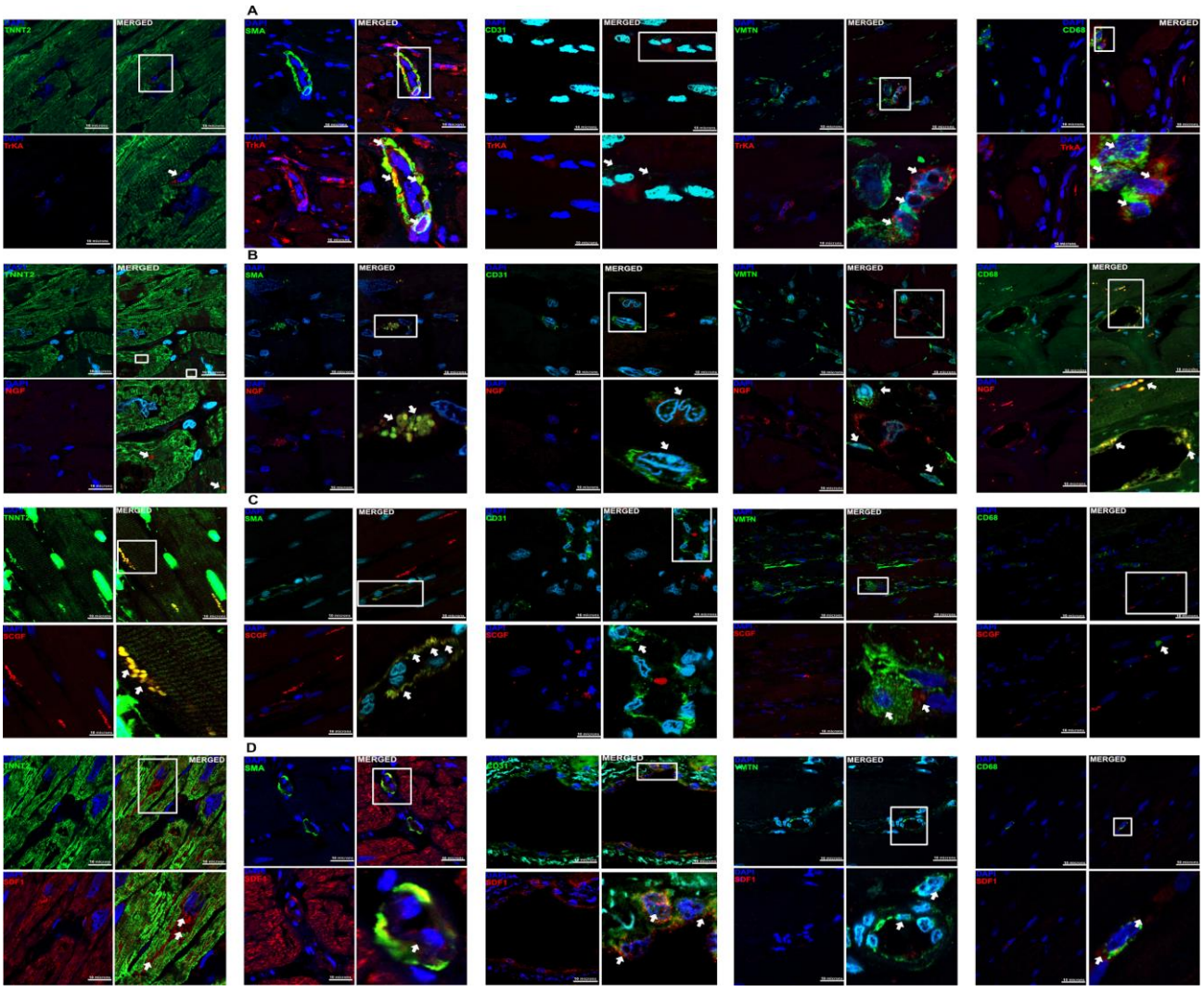

Figure E6. Gene expression of HGF, c-Met, NGF and SCGFb in the RV of pulmonary artery banding mice versus shams. Male C57BL/6 mice (12-14 weeks of age) were anaesthetized and PAB was performed with a non-absorbable silk suture. Five weeks after PAB surgery, right ventricular tissue was collected for gene expression analysis. The RNA expression of *Hgf, c-Met and Ngf* were significantly increased whereas the expression of *Scgfβ* was significantly decreased in right ventricular homogenates from PAB compared to Sham control mice. Data are presented as mean±SEM (n=4/group). Student's 2-tailed, unpaired t-test.

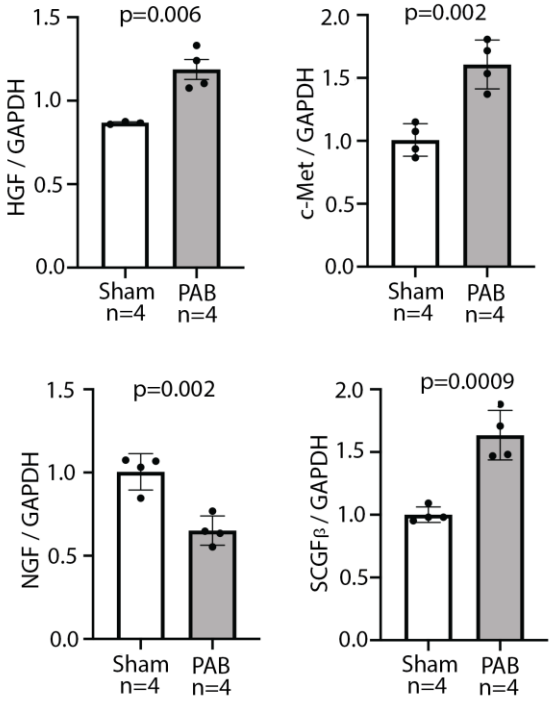

Table E1. Circulating proteomic biomarkers assessed in the study using flow cytometry multiplex arrays (Luminex®). PAH: pulmonary arterial hypertension; PH: pulmonary hypertension.

Abbreviation	Full name	Selected features
Interleukins and receptors		
IL1α	Interleukin-1 alpha	- Pro-inflammatory cytokine - Produced by macrophages, neutrophils and endothelial cells - Induced TNFα release by endothelial cells - Stimulates hepatocytes for CRP secretion - Binds to the interleukin-1 receptor
IL1β	Interleukin-1 beta	- Produced by activated macrophages as a proprotein, which is proteolytically processed to its active form from caspase 1 - Cell proliferation, differentiation and apoptosis
IL2	Interleukin-2	- Promotes the differentiation of immature T-cells into regulatory T-cells, effector T-cells or memory T-cells
IL3	Interleukin-3	- Stimulates proliferation of all cells in the myeloid lineage
IL4	Interleukin-4	- Induces the differentiation of naïve helper T-cells (Th0 cells) to Th2 cells - Decreases the production of Th1 cells and macrophages, promotes M2 repair macrophages > M1
IL5	Interleukin-5	- Produced by type-2 T helper cells and mast cells - Associated with eosinophil and allergy
IL6	Interleukin-6	- Acts as both a pro-inflammatory cytokine (secreted by macrophages and stimulating acute phase protein synthesis and production of neutrophils) and an anti-inflammatory myokine (through inhibitory effects on TNF-alpha and IL-1, and activation of IL-1ra and IL-

		10)
LIF	Leukemia inhibitory factor	- Interleukin-6 class cytokine - Affects cell growth by inhibiting differentiation - Role in cachexia and inflammation
IL7	Interleukin-7	- Hematopoietic growth factor, role in lymphocyte maturation
IL9	Interleukin-9	- Secreted by CD4+ helper cells that acts as a regulator of a variety of hematopoietic cells - Stimulates cell proliferation and prevents apoptosis
IL10	Interleukin-10	- Anti-inflammatory cytokine
IL12p70 IL12p40	Interleukin-12 (p70=active heterodimer) (p40=homodimer)	- Produced by dendritic cells, macrophages, and neutrophils - Promotes the differentiation of naive T cells into Th1 cells, involved in the activation of NK cells and T-cells - Stimulates production of IFNγ and TNFα - Anti-angiogenic activity
IL13	Interleukin-13	- Involved in allergic inflammation
IL15	Interleukin-15	- Secreted by mononuclear phagocytes - Induces cell proliferation of NK cells
IL16	Interleukin-16	- Pleiotropic cytokine that functions as a chemoattractant and a modulator of T cell activation
IL17	Interleukin-17	- Proinflammatory cytokine, acts in synergy with IL1 and TNFα
IL18	Interleukin-18	- Proinflammatory cytokine - Produced by macrophages and other cells
IL1Rα	Interleukin-1 receptor alpha chain	- Secreted by immune and epithelial cells - Natural inhibitor of the pro-inflammatory effect of IL1β
IL2Rα	Interleukin-2 receptor alpha	- Transmembrane protein present on activated T-cells and B-cells

	chain	- Soluble form elevated in T-cell lymphoma/leukemia used for disease monitoring.
Chemokines		
MCP1 = CCL2	Chemokine (C-C motif) ligand 2	- Recruits monocytes, memory T cells, and dendritic cells to the sites of inflammation - Implicated in the pathogenesis of atherosclerosis, CTEPH
MIP1α = CCL3	Chemokine (C-C motif) ligand 3	- Produced by macrophages after stimulation by bacterial endotoxin - Activates granulocytes (neutrophils, eosinophils and basophils) leading to acute neutrophilic inflammation - Induces secretion of IL-1, -6 and TNF-α from fibroblasts and macrophages
MIP1β = CCL4	Chemokine (C-C motif) ligand 4	- Idem than CCL3.
RANTES = CCL5	Chemokine (C-C motif) ligand 5	- Recruits T cells, eosinophils, and basophils, - Plays an active role in recruiting leukocytes into inflammatory sites
MCP3 = CCL7	Chemokine (C-C motif) ligand 7	- Specifically attracts monocytes, and regulates macrophage function
CTACK = CCL27	Chemokine (C-C motif) ligand 27	- Plays a role in T-cell mediated inflammation of the skin - Elicits chemotactic effect by binding to the chemokine receptor CCR10
Eotaxins	Chemokine (C-C motif) ligand 11, 24, 26	- Recruits eosinophils
GROa = CXCL1	Chemokine (C-X-C motif) ligand 1	- Expressed by macrophages, neutrophils and epithelial cells - Has neutrophil chemoattractant activity, is involved in angiogenesis, inflammation

		- Has his action through receptor CXCR2
IL8 = CXCL8	Chemokine (C-X-C motif) ligand 8 = Interleukin-8	- Produced by macrophages and endothelial cells - Has neutrophil chemoattractant activity and potently promotes angiogenesis
MIG = CXCL9	Chemokine (C-X-C motif) ligand 9	- Chemoattractant for T-cells
IP10 = CXCL10	Chemokine (C-X-C motif) ligand 10	- Chemoattraction for monocytes/macrophages, T cells, NK cells, and dendritic cells - Promotes T cell adhesion to endothelial cells - Inhibits bone marrow colony formation and angiogenesis
SDF1a = CXCL12	Chemokine (C-X-C motif) ligand 12	- Has lymphocyte chemoattractant activity - Role in angiogenesis - Associated with risk of coronary disease
Growth factors		
MCSF = CSF1	Macrophage colony-stimulating factor = Colony stimulating factor 1	- Hematopoietic growth factor involved in the proliferation, differentiation, and survival of monocytes, macrophages, and bone marrow progenitor cells - Involved in the development and progression of atherosclerosis
NGF	Nerve growth factor	- Involved in the growth, maintenance, proliferation, and survival of neurons - Role in the regulation of the immune system - Released in high concentrations by mast cells, playing a role in pain perception in areas under inflammation - Released by CD4+ T cell clones, inducing a cascade of maturation of T cells under infection - The expression of NGF is increased in inflammatory diseases such as asthma where it suppresses

		inflammation - Role in cardiovascular disease (reduced levels of NGF in acute coronary syndromes) - Increased in the right ventricle of mice with PH model
SCF	Stem cell factor	- Role in hematopoiesis - Cardiomyocyte-specific overexpression of transmembrane SCF promotes stem cell migration and improves cardiac function and animal survival after myocardial infarction
SCGFβ	Stem cell growth factor beta	- Hematopoietic growth factors
TNFα	Transforming growth factor alpha	- Mainly produced by activated macrophages - Proinflammatory cytokine - Promotes the development of PAH by reducing BMPR2 expression, promoting BMPR-II cleavage in vascular cells, and driving inappropriate proliferation of smooth muscle cells in pulmonary arteries
TNFβ	Transforming growth factor beta 1	- Role in immunoregulation - Negative autocrine growth factor
HGF	Hepatic growth factor	- Paracrine factor normally produced by cells of mesenchymal origin (fibroblasts, macrophages) - Role in normal embryogenesis and development, and in adults, role in tissue repair - Cardioprotective properties reported in the left heart - High circulating associated levels in left pressure overloaded disease and left heart failure
PDGFbb	Platelet-derived growth factor bb	- Role in angiogenesis - Produced by platelets upon activation, smooth

		muscle cells, activated macrophages, and endothelial cells
FGF2 = FGFβ	Basic fibroblast growth factor	- Mitogenic, involved in cell survival activities and angiogenesis
GCSF	Granulocyte colony-stimulating factor	- Stimulates the bone marrow to produce granulocytes and stem cells and release them into the bloodstream - Stimulates the survival, proliferation, differentiation, and function of neutrophils precursors and mature neutrophils
GMCSF	Granulocyte-macrophages colony-stimulating factor	- Secreted by macrophages, T cells, mast cells, natural killer cells, endothelial cells and fibroblasts - Promotes neutrophil, macrophages and eosinophil proliferation and maturation
VEGF-A	Vascular endothelial growth factor-A	- Role in angiogenesis and vasodilation - Chemotactic for granulocytes and macrophages
Other cytokines		
MIF	Macrophage migration inhibitory factor	- Proinflammatory cytokine - Involved in cell-mediated immunity, immunoregulation, and inflammation - In PAH: elevated concentrations of MIF - In mouse models of PH: antagonism of MIF inihibits hypoxia-induced smooth cell proliferation
TRAIL	TNF-related apoptosis-inducing ligand	- Induces apoptosis
IFNA2	Interferon alpha-2	- Potent antitumor activity, activation of the immune system which can eliminate tumor cell
IFNγ	Interferon gamma	- Important role for innate and adaptive immunity against viral, bacterial and protozoal infections - Activator of macrophages and MHC II

Table E2. Right heart risk scores. Mayo Clinic derived-score and Stanford-derived score for prediction of death, lung transplant or admission at 3 years in the recently published Vera Moulton Wall Center cohort (3).

Mayo Clinic score		**Stanford score**	
Variables	Points	Variables	Points
RV longitudinal strain (%)		RV end-systolic remodeling index	
≥25 (reference)	0	<1.32 (reference)	0
[20 – 25[	3	[1.32 - 1.45[	2
[15 – 20[	5	[1.45 - 1.60[	3
<15	5	≥1.60	5
NT-proBNP (pg/mL)		NT-proBNP (pg/mL)	
< 1500	0	< 1500	0
≥ 1500	1	≥ 1500	2
NYHA class		NYHA class	
I or II	0	I or II	0
III or IV	3	III or IV	3
Total	/17	Total	/15

NYHA: New York Heart Association; RV: right ventricular.

Table E3. REVEAL PAH Risk Score. *Adapted from Benza et al. Circulation, 2010.*

Variables	
WHO Group I Subgroup	APAH-Connective Tissue Disease: +1 APAH-Portal Hypertension: +2 Familial-PAH: +2
Demographics and Comorbidities	Renal Insufficiency: +1 Males Age > 60years: +2
NYHA/WHO Functional Class	I: -2 III: +1 IV: +2
Vital Signs	Systolic Blood Pressure <110mmHg: +1 Heart Rate > 92bpm
6-Minute Walk Test	> or = 440m: -1 < 165m: +1
BNP levels	< 50pg/mL: -2 > 180 pg/mL: +1
Echocardiogram	Pericardial Effusion: +1
Pulmonary Function Test	% predicted DLCO > or =80: -1 % predicted DLCO < or =32: +1
Right Heart Catheterization	Mean Right Atrial Pressure > or =20mmHg within 1 year: +1 Pulmonary Vascular Resistance >32 Wood units: +2

Table E4. Characteristics of the patients with pulmonary arterial hypertension (PAH) from which right ventricular biopsies were obtained.

	Age (years)	**Sex**	**PH etiology**	**NYHA class**	**MPAP (mmHg)**	**Preoperative PH-specific therapy**
Patient 1	43	Male	Eisenmenger (Atrial Septal Defect)	III	51	PDE5I, ERB, treprostinil
Patient 2	24	Female	Drug and Toxin	III	50	PDE5I, ERB, prostacyclin
Patient 3	61	Female	Idiopathic	IV	59	PDE5I, ERB, treprostinil
Patient 4	52	Female	BMPR2 mutation	III	64	PDE5I, ERB, prostacyclin

ERB: endothelin receptor blocker; MPAP: mean pulmonary arterial pressure; NYHA: New York Heart Association functional class; PDE5I: phosphodiesterase inhibitor; PH: pulmonary hypertension.

Table E5. Biomarkers with significant partial least square regression coefficients for association with right heart metrics.

	High cytokine level associated with "unfavorable" metric		**High cytokine level associated with "favorable" metric**	
	Discovery	Validation	Discovery	Validation
Mayo right heart score	**SCGF**β **HGF** **NGF** MCSF SDF1a MIG	**HGF** **SCGF**β **NGF**	TRAIL IL2Rα	None
Stanford right heart score	**SCGF**β **HGF** **NGF** SDF1a Eotaxin	**SCGF**β **HGF** **NGF** VEGF	None	None
RVLS	**SCGF**β **HGF** SDF1a **NGF**	**HGF** **SCGF**β **NGF**	PDGFβ GMCSF TNFα	None
RVESRI	**HGF** **SCGF**β **NGF**	**SCGF**β **HGF**	PDGFβ IL3 GCSF	None

	MCP1 Eotaxin			
NT-proBNP (log)	**HGF** **SCGF**β **NGF** MIG SDF1a	**HGF**	TRAIL ILR2α PDGFβ LIF IL3 MCP3	None
NYHA class	**HGF** **SCGF**β MIG MCSF	None	None	None
MPAP	None	None	MCP3	None
PVR	None	None	SCF	SCF IL12

P values <0.05 using Jacknife test were considered significant. MPAP: mean pulmonary arterial pressure; PVR: pulmonary vascular resistance; NT-proBNP: N-terminal pro-b type natriuretic peptide; NYHA: New York Heart Association; RVESRI: right ventricular end-systolic remodeling index; RVLS: right ventricular free-wall longitudinal strain. For circulating biomarkers abbreviations, please see **Table E1**.

Table E6. Multivariable Cox regression analysis models for prediction of the primary end point (death, transplant or readmission for heart failure) at 3 years in the total PAH cohort (n=197).

Variables were entered in the model using enter mode. The Mayo right heart score was based on the New York Heart Association class, NT-proBNP and right ventricular longitudinal strain (RVLS). The Stanford right heart score was based on the New York Heart Association class, NT-proBNP and right ventricular end-systolic remodeling index (RVESRI). The REVEAL score was based on the Registry to Evaluate Early And Long-term PAH Disease Management (REVEAL) groups: low, average, moderate high, high, very high. HGF: hepatic growth factor; NGF: nerve growth factor; SCGFβ: stem cell growth factor beta and SDF1: stromal cell-derived factor 1.

	Unadjusted Hazard ratio	95% confidence interval	p value	$\chi 2$	-2Log Likelihood	p value
REVEAL score-based models						
Model 1				46.47	357.77	<0.0001
REVEAL score	1.52	1.33; 1.73	<0.0001			
Model 2				52.96	353.20	<0.0001
REVEAL score	1.45	1.26; 1.67	<0.0001			
HGF	1.01	1.01; 1.02	0.03			
Model 3				50.80	354.10	<0.0001
REVEAL score	1.57	1.37; 1.79	<0.0001			
NGF	0.99	0.99; 1.01	0.07			
Model 4				47.22	357.41	<0.0001
REVEAL score	1.53	1.34; 1.76	<0.0001			
SCGFβ	0.99	0.99; 1.00	0.56			

Model 5				44.69	356.88	<0.0001
REVEAL score	1.54	1.35; 1.76	<0.0001			
SDF1	0.99	0.99; 1.00	0.36			
Stanford score-based models						
Model 1				34.00	370.78	<0.0001
Stanford score	1.36	1.22; 1.52	<0.0001			
Model 2				45.50	364.13	<0.0001
Stanford score	1.28	1.14; 1.45	<0.0001			
HGF	1.01	1.01; 1.02	<0.01			
Model 3				35.63	369.31	<0.0001
Stanford score	1.38	1.23; 1.55	<0.0001			
NGF	0.99	0.99; 1.00	0.25			
Model 4				34.28	369.98	<0.0001
Stanford score	1.40	1.23; 1.58	<0.0001			
SCGFβ	0.99	0.99; 1.00	0.39			
Model 5				34.11	370.68	<0.0001
Stanford score	1.37	1.22; 1.53	<0.0001			
SDF1	1.00	0.99; 1.00	0.36			
Mayo score-based models						
Model 1				27.69	373.05	<0.0001
Mayo score	1.67	1.35; 2.07	<0.0001			
Model 2				43.31	363.23	<0.0001
Mayo score	1.53	1.24; 1.88	<0.0001			
HGF	1.01	1.00; 1.01	0.001			
Model 3				28.36	371.83	<0.0001
Mayo score	1.72	1.38; 2.15	<0.0001			
NGF	0.99	0.99; 1.00	0.29			

Model 4				27.79	373.05	<0.0001
Mayo score	1.67	1.34; 2.09	<0.0001			
SCGFβ	1.00	0.99; 1.00	0.97			
Model 5				27.69	373.01	<0.0001
Mayo score	1.68	1.35; 2.08	<0.0001			
SDF1	1.00	0.99; 1.00	0.83			

References

1. Amsallem M, Sweatt AJ, Aymami MC, Kuznetsova T, Selej M, Lu H, Mercier O, Fadel E, Schnittger I, McConnell MV, Rabinovitch M, Zamanian RT, Haddad F. Right Heart End-Systolic Remodeling Index Strongly Predicts Outcomes in Pulmonary Arterial Hypertension: Comparison With Validated Models. Circ Cardiovasc Imaging 2017; 10.
2. Boehm M, Tian X, Mao Y, Ichimura K, Dufva MJ, Ali K, Prosseda SD, Shi Y, Kuramoto K, Reddy S, Kheyfets VO, Metzger RJ, Spiekerkoetter E. Delineating the molecular and histological events that govern right ventricular recovery using a novel mouse model of PA de-banding. Cardiovasc Res 2019;doi:10.1093/cvr/cvz310.
3. Mevik BH and Wehrens R. The pls package: Principal component and partial least squares regression in R. Journal of Statistical Software, 18:1–24, 2007.
4. Mevik BH and Cederkvist HR. Mean squared error of prediction (MSEP) estimates for principal component regression (PCR) and partial least squares regression (PLSR). Journal of Chemometrics, 18:422–429, 2004.